Global NEST Journal, Vol 26, No 7, 06199

The photocatalytic performance of Co_3O_4/Na-alginate nanocomposite for the dynamic removal of direct red 31 dye: degradation and mechanical pathways

Saba Naz[1], Shumaila Kiran[1]*, Tahsin Gulzar[1] and Tahir Farooq[1]
[1]Department of Applied Chemistry, Government College University, Faisalabad, 38000, Pakistan
Received: 24/05/2024, Accepted: 07/07/2024, Available online: 10/07/2024
*to whom all correspondence should be addressed: e-mail: shumaila.asimch@gmail.com
https://doi.org/10.55555/gnj.006199

Graphical abstract

Abstract

This study examines the use of Co_3O_4 nanocomposite as a photo-catalyst in an aqueous solution for photocatalytic degradation of dyes under U.V. It has been observed that substrate concentrations, catalyst, pH, oxidant present and temperature affect dye degradation. The characterization of synthesized Co_3O_4 NPs and Co_3O_4/Na-Alg NC was done using UV-visible, S.E.M., XRD, and FTIR. Co_3O_4 NPs and Co_3O_4/Na-Alg NC were found to be 23 nm and 10 nm in size, respectively. The synthesized Co_3O_4/NaAlg NC were employed to degrade Direct Red 31 dye using batch experiments by optimization of experimental conditions. Eighty minutes were given to the experiment. At ideal conditions, including 0.02% dye, three mg/L Co_3O_4/NaAlg NC photocatalyst, 0.03 mM H_2O_2, pH 5, and 70°C temperature, the maximum degradation (68.24%) was achieved. T.O.C. and C.O.D. were evaluated to check the proficiency of this process. It was found that the percentage reduction in T.O.C. and C.O.D. was 66.7% and 65.2%. The generation of non-toxic products was validated by the Direct Red 31 dye degradation route. The study concluded that the synthesized nanocomposites could be chosen for the remediation of dyes-containing wastewater. Because it is economical and environmentally beneficial, the produced Co_3O_4/Na-Alg NC is strongly advised for dye degradation.

Keywords: Co-precipitation, Co_3O_4/Na-Alginate nanocomposite, characterization, direct red 31 dye degradation, photocatalysis, kinetic and mineralization study.

1. Introduction

Dyes are significant industrial commosssdities, as the majority of dyes' by-products are released into the environment, which significantly contributes to environmental damage. Without any additional treatment, the textile and paper sectors discharge large amounts of these non-biodegradable, carcinogenic pollutants into the water, so contaminating the water (Kumar *et al.* 2023). These hues can cause cyanosis, jaundice, shock, increased heart rate, vomiting, tissue necrosis, and quadriplegia, among other harmful effects in people (Waliullah *et al.* 2023). Due to their complex structure, pigments accumulate in water and block sunlight penetration, preventing sequential photosynthesis. As a result, dye pollution is recognized as a serious issue, which motivates authorities to act and create effective remediation techniques. Various methods are used to get rid of dye pollution (Kiran *et al.* 2017). They are coagulation/flocculation (Hadadi *et al.* 2023), ion exchange (Raji *et al.* 2023), membrane filtration (Sheikh *et al.* 2023), electrocoagulation (Negash *et al.* 2023), ozonation (Lanzetta *et al.* 2023), Fenton process (Eskikaya *et al.* 2023), photocatalytic degradation (Matei *et al.* 2023) and adsorption process (Waliullah *et al.* 2023). There are a number of disadvantages to treating wastewater containing textile dye using conventional chemical, physical, and biological processes, including high treatment costs, high energy requirements, and the creation of secondary contaminants (Kiran *et al.* 2018; Bano *et al.* 2024; Bhutto *et al.* 2024).

In this regard, the application of transition metal nanoparticles has gained traction (Krishnan *et al.* 2023).

Transition metal oxide nanoparticles with a suitable band gap and flat band potential energy levels are the main components of photocatalysts. The use of transition metal oxide nanoparticles to treat effluent containing dangerous dyes has also achieved high popularity (Mahdiani *et al.* 2018; Maniammal *et al.* 2018; Dammala *et al.* 2019; Sujatha *et al.* 2019). Their unique photocatalytic property is associated with their large surface area and semiconducting characteristics (Roy *et al.* 2023). The synthesis of transition metal oxides at the nanoscale with varying morphologies is highly desirable because of their unique properties, which are dependent on their structure, morphology, dimension, and size distribution in addition to their chemical composition (Wu *et al.* 2020; Yin and Hasegawa, 2023; Al-Askar *et al.* 2023). The transition metal nanoparticles' qualities like magnetic, electronic, and optical qualities (Mayakkannan *et al.* 2023), have made it possible to be successfully applied over a wide range of applications comprising lithium-ion batteries (Hu *et al.* 2023; Elsharawy *et al.* 2023; Akram *et al.* 2024), sensors (Yao *et al.* 2023), and catalysis (Tyagi *et al.* 2020; Akram *et al.* 2023). Numerous transition metals and their oxide nanostructures have been synthesized and studied, including cobalt (Kharat *et al.* 2023), iron (Tai *et al.* 2023), zinc (Al-Enizi *et al.* 2023), copper (Obisesan *et al.* 2019), etc. Among these, Co3O4, in particular, exhibited an amazing track record of wide-ranging applications for dyes, catalysts, gas sensors, and energy storage materials, as well as magnetic compounds (Vinayagam *et al.* 2023). The Co-based nanostructures have been considered due to their unbeatable and novel physiochemical properties. Co_3O_4 is a p-type semiconductor that has a narrow band gap (1.2–2.1 eV), good thermal and chemical stability, low solubility, and intriguing electrical, magnetic, and catalytic properties (Yousefi *et al.* 2021; Kumarage and Comini, 2021). Co_3O_4 can be used as a photocatalyst or co-catalyst for visible-light-driven photocatalytic reactions because of its exceptional qualities (Chang *et al.* 2020; Ghobadifard *et al.* 2023). In order to synthesize nanocomposites for wastewater treatment, nanomaterials have been added to polymeric materials. Moreover, adding these inorganic components to a polymeric matrix can improve the photocatalytic function of the nanocomposite materials (Makhado *et al.* 2019b; Akram *et al.* 2021).

Alginate is a naturally occurring polymer obtained from brown algae. It is made up of a linear polymer with different ratios of β-L-guluronate (G) and β-D-mannuronate (M) units. Alginate has drawn interest because of its many uses, porosity, and surface area, and it is s stable in many organic solvents (Sellimi *et al.* 2015; Hecht and Srebnik, 2016). It is appropriate for use as an immobilization matrix in the treatment of wastewater. Moreover, because of the presence of negative carboxylate functionalities along its polymeric chains, it possesses endearing qualities, including ion selectivity, high affinity, and binding ability for cations (Shen and Wang, 2014; Lin *et al.* 2023; Alavinia *et al.* 2023).

For the first time ever, a cobalt oxide/alginate nanocomposite (Co_3O_4/Na-Alg NC) was created in this study to help degrade the Direct Red 31 dye (D.R. 31 dye) under U.V. light. This study involved the synthesis of Co_3O_4 nanoparticles by the co-precipitation method and was incorporated in a sodium alginate matrix to form a cobalt oxide/sodium alginate nanocomposite (Figure 1). Cobalt oxide/alginate nanocomposite (Co_3O_4/Na-Alg NC) was applied for the photo-degradation of the D.R. 31 dye.

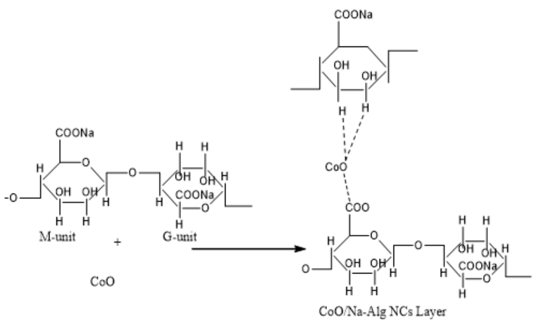

Figure 1. Reaction for the synthesis of Cobalt oxide/Na-alginate bio-nanocomposite

2. Material and methods

All of the chemicals were taken from the Nadeem Scientific and Chemical store in Faisalabad, Punjab, Pakistan. Cobalt chloride, sodium alginate, Sodium hydroxide (NaOH), Hydrogen peroxide (H_2O_2, 35%), sulphuric acid (H_2SO_4). Direct Red 31 dye (D.R. 31 dye) was supplied by the Dyes and Chemicals store in Faisalabad, Punjab, Pakistan. All chemicals used in this study were pure and used as such. All experiments were conducted with distilled water (D.W.).

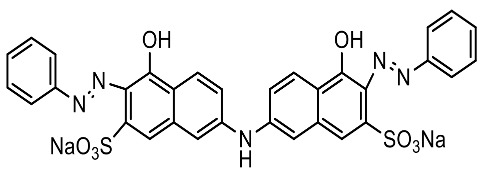

Figure 2. Structure of Direct Red 31 dye (C.I. 29100)

2.1 Synthesis of Co_3O_4 nanoparticles (Co_3O_4 NPs)

Co_3O_4 nanoparticles (Co_3O_4 NPs) were synthesized following Samer *et al.* (2022) via co-precipitation method with modifications where required. 50 mL NaOH solution (4 M) into 50 mL of $CoCl_2.6H_2O$ solution (0.2 M) at an approximate rate of 5 mL/min in strong mixing conditions (1500 rpm). The stirring of the mixture continued for 4 hours. The precipitates were collected, filtered, rinsed with deionized water and filtered and dried in an oven at 100°C. To get a homogeneous powder, the dry precipitates were ground using an agar mortar. The calcination of the resulting powder was done for five hours at 200°C (Figure 3) (Samer *et al.* 2022).

2.2 Synthesis of Cobalt oxide/Na-alginate nanocomposite (Co_3O_4/Na-Alg NC)

The cobalt oxide/Na-Alginate nanocomposite (Co_3O_4/Na-Alg NC) was prepared using Helmiyati and Wahyuningrum's method (2018) with slight modifications.

An aqueous sodium alginate solution was formed by dissolving the sodium alginate in distilled water with continuous stirring for four hours at room temperature. In this solution, Co_3O_4 NPs were added (prepared by the above Scheme) and stirred at 500 rpm for one hour, then the solution was set to ultra-sonication for 30 min for homogenization. The amount of sodium alginate and Co_3O_4 NPs in a 1:1 ratio was used in the experiment. Finally, the resulting Co_3O_4/Na-Alg NC was taken out, dried and used for further experimental characterization (Figure 4) (Helmiyati and Wahyuningrum 2018).

Figure 3. Synthesis of cobalt oxide nanoparticles with Scheme

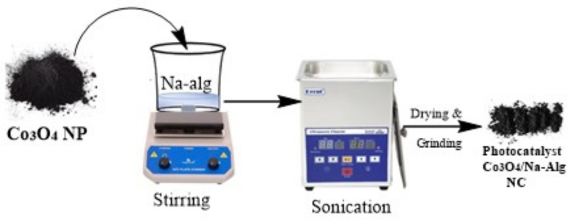

Figure 4. Co_3O_4 Synthesis of cobalt oxide/Na-alginate nanocomposite (Co_3O_4/Na-Alg NC)

2.3 Characterization of Co_3O_4 NPs and Co_3O_4/Na-Alg NC

The synthesized Co_3O_4 nanoparticles (Co_3O_4 NPs) and Co_3O_4/sodium alginate nanocomposite (Co_3O_4/Na-Alg NC) were characterized by optical, structural and elemental techniques. The optical properties were determined by employing U.V.–visible spectroscopy. With an STA-4300 spectrophotometer operating at room temperature, the Co_3O_4 nanoparticles' U.V.–visible absorption spectra were captured. To create a homogenous suspension, the sample for the UV-Vis investigations was thoroughly mixed in distilled water using sonication for ten minutes. Scanning electron microscopy was used to assess the size and shape of the surface. The structural properties were analyzed by employing powder X-ray diffraction. Elemental analysis and chemical compositions were examined by Fourier Transform Infrared Spectroscopy (Khalaji *et al.* 2019). The sample was powdered and used for S.E.M., XRD, and FTIR.

2.4 Decolourization of D.R. 31 dye using Co_3O_4/Na-Alg NC as photocatalyst

2.4.1 Determination of λmax for D.R. 31 dye

For scanning of λmax, a dye solution was made, and a double beam U.V.–vis spectrophotometer was used to measure absorbance.

2.4.2 Experimental procedure with optimization of reaction variables

Firstly, the dye was used, whose 0.01% solution was prepared in water. The dye solution was taken in a reaction flask, and pH was adjusted to 5 using 0.1M NaOH/0.05M H_2SO_4. Then, 4mg of cobalt oxide/Na-alginate nanocomposite was added to the reaction flask having D.R. 31 dye solution. The reaction flask was kept on a hot plate with a magnetic stirrer at 40 ℃ operating under a UV lamp, and the reaction was allowed to let run for 80 minutes. The reaction progress was checked by taking out a small amount of reaction aliquot from the reaction mixture after each 10 minutes and noting its absorbance value at λ_{max} using the U.V./Vis spectrophotometer (STA-4300).

The D.R. 31 dye level was varied from 0.01-0.06%, concentration of sodium alginate-based metal oxide nanocomposite from 1-6 mg, H_2O_2 from 0.01-0.05 mM, reaction time from 10-70 min, pH from 5-10 and temperature range from 30°C - 80°C (Patra *et al.* 2022).

2.4.3 Chemical analysis

The following formula was used to determine the efficiency of dye removal:

Decolorization (%) = (I – F)/I × 100

Where I denote the dye solution's starting absorbance and F its final absorbance (Kiran *et al.* 2020), the UV-Vis spectrophotometer was utilized to check the dye solution's absorption.

2.4.4 Statistical analysis

Three runs of the sample through the device were performed. The findings are produced using the average value (Steel *et al.* 1997).

2.4.5 Degradation pathway

By rupturing the older bonds, the dye was broken down into intermediate products and then into end products, with the production of new products occurring in different steps, as illustrated in Figure 13 (Koli *et al.* 2018).

2.5 Mineralization study

Water quality metrics such as C.O.D. and T.O.C. were evaluated for both treated and untreated wastewater samples.

Calculating the C.O.D. required adding 1.5 mL of the digestion solution (made by dissolving 2.5 g $K_2Cr_2O_7$ and 8.3 g of $HgSO_4$ in 40 mL H_2SO_4 and diluting it to 250 mL with deionized water) and 3.5 mL of the catalyst solution (made by dissolving 5 g of Ag_2SO_4 in 500 mL of conc. H_2SO_4 and storing it for 48 hours). Then, each vial was filled with 2.5 mL of dye solution (treated and untreated). The blank sample was prepared using 2.5 mL of deionized water and all other components except dye. After that, the vials were heated to 150°C for 110 minutes. Following that, the vials were allowed to cool to room temperature, and the absorbance at 600 nm was noted (Rahmat *et al.* 2023).

In digesting vials, 1.6 mL of concentrated H_2SO_4, 4 mL dye solutions, and 1 mL (2N) $K_2Cr_2O_7$ solution were added and thoroughly mixed in order to determine T.O.C. The blank sample was prepared using 2.5 mL of deionized water and all other components except dye. After 90 minutes at 110°C in the oven, the flasks were chilled. The absorbance values were measured at 590 nm. The absorbance of a blank sample was subtracted from the sample's absorbance to get a reliable prediction of the sample's absorbance (Greenberg *et al.* 1985; Rahmat *et al.* 2023).

This formula was used to determine the C.O.D. and T.O.C. values:

SF × A = TOC⁄COD

Where S.F. denotes the standard factor, and A denotes the absorbance.

The standard factor's formula is

Standard factor = Conc. of standard ⁄ its absorbance

3. Results and discussion

3.1 Characterization of Co_3O_4 NPs and Co_3O_4/Na-Alg NC

The characteristic analysis of the Co_3O_4 NPs and Co_3O_4/Na-Alg NC was done using S.E.M., UV-Visible, XRD, and FTIR techniques. The results of the analysis are described below.

S.E.M. was used to examine the morphology of Co_3O_4 NPs and Co_3O_4/Na-Alg NC. The electrographs of the Co_3O_4 NPs and Co_3O_4/Na-Alg NC synthesized are shown in Figure 5. S.E.M. provides information about the size of nanoparticles and their homogeneity and size distribution. The uniform distribution of particles is indicated by the S.E.M. image. The spherical form, small size, and high surface energy of the synthesized N.P.s led to their aggregation and form of tiny clusters, as seen in Figure 5a. That's why it became difficult to calculate the size of nanoparticles individually. Using Image J software, the size distribution of these clusters was found. The size has varied from 400 nm to 700 nm, as we have seen. The individual particle size was calculated using XRD analysis. The results are supported by the literature (Lakra *et al.* 2021).

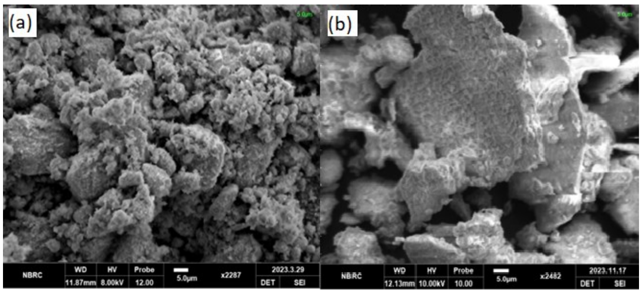

Figure 5. (a) S.E.M. of Co_3O_4 nanoparticles (b) S.E.M. of Co_3O_4/Na-Alg nanocomposite

Co_3O_4/Na-Alg NC images reveal a pore-filled, rough surface in Figure 5b. Particles in the sodium alginate matrix are evenly distributed, as seen by the Co_3O_4/Na-Alg NC Figure 5b. With the formation of Co_3O_4 nanoparticles on the surface, the morphology of Co_3O_4/Na-Alg NC altered to a more compact surface with wrinkles. This suggests that the polymeric matrix shrinks as a result of Co_3O_4 nanoparticle adsorption and creates a more compact structure. The surface morphology of Co_3O_4/Na-Alg NC changes as a result of the development of Co_3O_4 nanoparticles (Hai *et al.* 2016).

The results of UV-visible spectroscopy demonstrated that, as seen in Figure 6, the usual peaks of Co_3O_4 NPs were found in the maximal wavelength range between 200-350 nm and 380-600 nm**.** Figure 6 shows the UV–visible spectrum of the prepared Co_3O_4 NPs and Co_3O_4/Na-Alg NC. It is clear that Co_3O_4 NPs have absorption at 200 nm and 400 nm. The 300 nm and 420 nm peaks are visible in the Co_3O_4/Na-Alg NC. These peaks represented the methods by which Co (II) and Co (III) were transferred to oxygen, respectively (Farhadi *et al.* 2016; Attia and Abdel-Hafez, 2021).

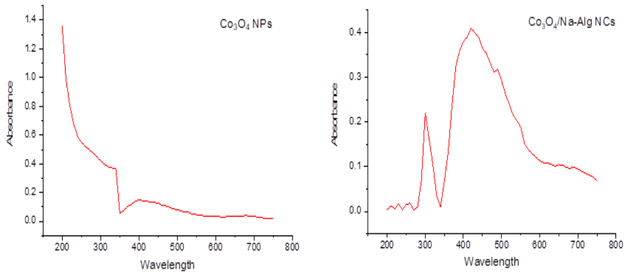

Figure 6. UV-visible of Co_3O_4 NPs and Co_3O_4/Na-Alg NC

XRD was used to examine the crystal structures and compositions of the Co_3O_4 NPs and Co_3O_4/Na-Alg NC, as seen in Figure 7. The diffraction peaks at 20.0°, 31.2°, 36.5°, 39.6°, 44.0°, 55.9°, 59.1°, and 65.2° were the present in Co_3O_4 NPs. These peaks may be correlated with the spinel Co_3O_4 characteristic peaks (JCPDS No. 43–1003). The crystal planes of spinel Co_3O_4 are represented by the peaks [111], [2 2 0], [3 1 1], [2 2 2], [4 0 0], [4 2 2], [5 1 1], and [4 4 0], in that order. After calcination, sharp peaks were seen, suggesting that good crystallization had been accomplished and that N.P.s and N.C.s had fully formed.

Since the material's full width at half-maximum (FWHM) and particle size are correlated, the peak corresponding to the [311] plane was selected for study. The FWHM values of the Co_3O_4 NPs and Co_3O_4/Na-Alg NC were determined to be 0.36145° and 0.8782°, respectively, using the Gaussian fitting model. The average particle size (D) of a material can be computed using Scherrer's equation as follows (Lakra *et al.* 2021; Samer *et al.* 2022).

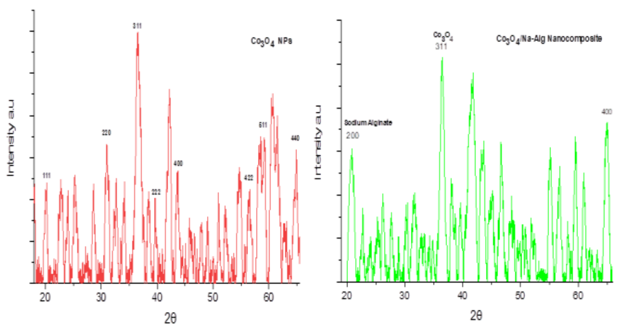

Figure 7. XRD patterns of Co_3O_4 Nanoparticles and Co_3O_4/Na-Alg Nanocomposites

$$D = \frac{0.9\lambda}{\beta \cos\theta}$$

Where θ is the diffraction angle (20.42° for N.P. and 36.48° for N.C.), β is the FWHM (Radian system), and l is the X-ray wavelength (0.154 nm). The Co_3O_4 NP and Co_3O_4/Na-Alg NC had average particle sizes of 23 and 10 nm, respectively**.** The particle size decreased when converted into nanocomposites. The literature has findings that are comparable (Fan *et al.* 2021).

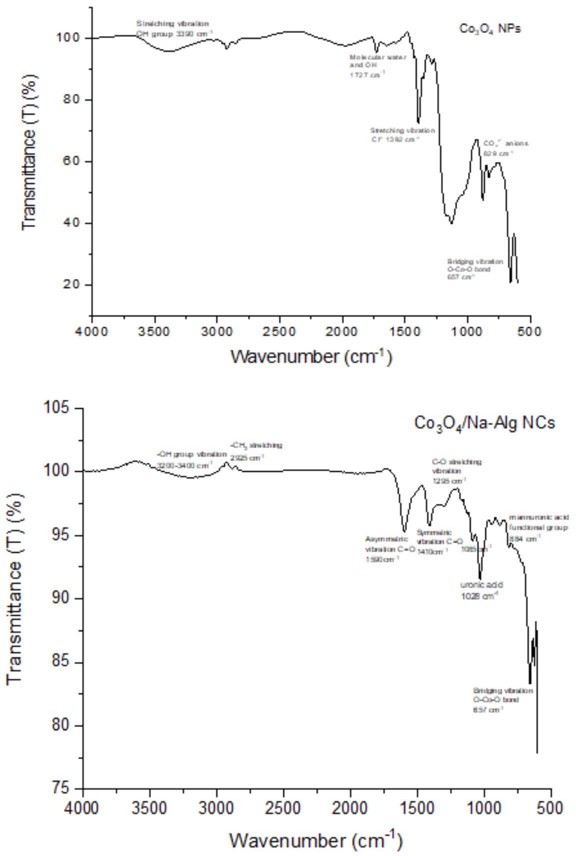

Figure 8. FTIR spectra of Co_3O_4 NPs and Co_3O_4/Na-Alg NC

The FTIR spectrum of Co_3O_4 NPs was captured in the wavenumber range of 600–4000 cm^{-1}. Figure 8 displays the Co_3O_4 NPs' FTIR spectrum. The stretching vibration mode of the O-H group is responsible for the broadband at 3390 cm^{-1}. Molecular water and O.H. are linked to the peak at 1727 cm^{-1} (Xu *et al.* 2015). The stretching vibration of Cl^{2-}, which is caused by the remaining cobalt chloride salt ($CoCl_2.6H_2O$), is represented by the peak at 1392 cm^{-1}. The distinctive peaks of CO_3^{2-} anions are linked to the band at about 829 cm^{-1} (Bhargava *et al.* 2018). The O-Co-O bond's bridging vibration was identified as the source of the absorption band at 657 cm^{-1}.

The FTIR spectra of Co_3O_4/Na-Alg NC revealed that the O-Co-O bond's bridging vibration was responsible for the absorption band at 657 cm^{-1}. The spectra showed the mannuronic acid functional group at wavenumber 884 cm^{-1} and the uronic acid at wavenumber 1028 cm^{-1}. The C-C and C.O.C. vibrations are also attributed to the strong and abrupt peak at 1028 cm^{-1}. The following peak, at approximately 1085 cm^{-1}, is linked with stretching vibrations of C–O, C–C, and C.O.C. The C-O stretching vibration was identified as the source of the bands at 1295 cm^{-1}. Asymmetric and symmetric C=O vibrations make up C.O.O.- stretching. At 1590 cm^{-1} for the first one and 1410 cm^{-1} for the second one. CH_2 stretching occurs at wavenumber 2928 cm^{-1} and O.H. functional group at wavenumber 3200-3400 cm^{-1} (Nastaj *et al.* 2016).

3.2 Determination of λ_{max} for D.R. 31 dye

The percentage and rate of degradation were calculated using the λ_{max} value. The absorbance of D.R. 31 dye (0.01%) was measured at 10 nm intervals from 340 to 750 nm in order to determine the wavelength with the highest absorption. λ_{max} was found to be 520 nm (Figure 9). The outcome is consistent with previous research (Abd El-Aziz *et al.* 2024).

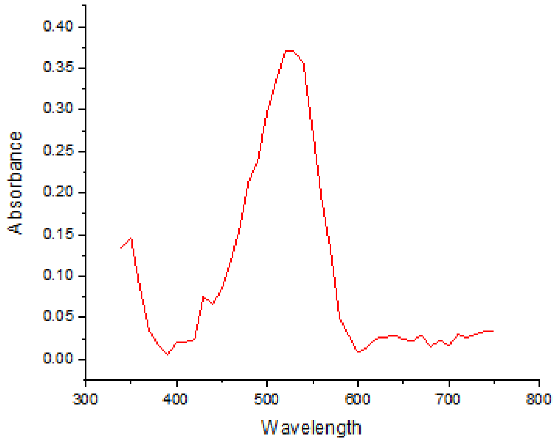

Figure 9. Scanning of λmax for Direct Red 31 dye

3.3 Optimization of experimental factors for photodegradation of D.R. 31 dye using Co_3O_4/Na-Alg NC

The experimental factors affecting D.R. 31 dye's rate of decolourization are the concentration of D.R. 31 dye (0.01–0.06%), the concentration of the nanoparticles (1–6 mg), H_2O_2 (0.01-0.05 %), pH (4–8), temperature (40–80°C) etc.

3.3.1 Effect of D.R. 31 dye different concentrations

The concentration of a dye is a significant factor in this treatment using an appropriate catalyst as it is directly linked with proficiency in the reaction. By adjusting the concentration within the range of 0.01% to 0.06%, the impact of D.R. 31 dye concentration on photodegradation was investigated. In these experiments, an initial catalyst dose of 4mg was added, the pH was adjusted to 5.0, and the temperature was set to 40°C for the 80-minute duration of the reaction. The findings showed, in Figure 10a, that from 0.01 to 0.02 % dye concentration, photocatalytic degradation of D.R. 31 dye was increased to 56.73% and that when the concentration of D.R. 31 dye increased from 0.02 to 0.06%, rate of dye decomposition reduced. D.R. 31 dye was therefore optimized at a concentration of 0.02%. This could be explained by the fact that at greater dye concentrations, less light reaches the photocatalyst surface, which lowers the concentration of reactive radicals produced by light and, ultimately, lowers the photocatalytic activity at higher starting dye concentrations (Elashery *et al.* 2023; Kiran *et al.* 2018). Moreover, self-association and clumping can occur when more dye particles are present, preventing dye particles from accessing the available catalytic region. Thus, the excess dye molecules and intermediates poisoned the photocatalysts active sites at high dye concentrations, reducing the efficacy of dye removal. The conclusions are consistent with the literature (Gola *et al.* 2021; Ghaffar *et al.* 2021).

3.3.2 Effect of photocatalyst Co_3O_4/Na-Alg NC different concentrations

It studied how different catalyst concentrations, ranging from 1 mgL^{-1} to 6 mgL^{-1}, affected the decolourization of D.R. 31 dye. The percentage of decolourization was used to optimize the amount of catalyst. Since the optimized concentration of D.R. 31 dye was 0.02 %, these parameters were used in the studies: pH at 5.0 and the temperature at 40°C was adjusted for the 80 minutes of reaction. When the catalyst concentration was changed from 1 mgL^{-1} to 3 mgL^{-1}, a degradation percentage of 59.64% was recorded. As the concentration increased from 4 mgL^{-1} to 6 mgL^{-1}, the catalyst's efficiency reduced. According to these experimental findings, three mgL^{-1} catalyst is the ideal reaction condition (optimal dose) for D.R. 31 dye in order to maximize efficiency. The catalyst quantity was adjusted while maintaining a constant dye concentration, and the resulting degradation plot is shown in Figure 10b. Hydroxyl radicals (O.H.) and reactive oxygen species (R.O.S.) are created in greater quantities when the number of catalytic species grows, and this causes the formation of electron-hole pairs to occur at a higher magnitude. That's why dye degradation is typically increased (Shokoohi *et al.* 2021). The improved efficiency of the nanocomposite for the dye up to 3 mgL^{-1} was visible in the current study. As shown in Figure 10b, raising the amount of the photo-catalyst from 4 mgL^{-1} to 6 mgL^{-1} does not significantly increase dye adsorption. This indicates that additional loading of the catalyst does not increase the photo-degradation efficacy because of increased suspension turbidity, inadequate light penetration, increased light scattering, or the adsorption and sedimentation of nanocomposites (Karim *et al.* 2021). This is consistent with the body of previously published research (Akhter *et al.* 2023).

3.3.3 Effect of H_2O_2 different concentrations on Photo-degradation

The transformation process of organic toxic effluents into non-toxic compounds is mainly linked with reactive oxidant species (R.O.S.). The impact of H_2O_2 on dye degradation was examined while holding all other parameters constant, such as the dye concentration at 0.02%, the catalyst concentration (nanocomposite) at 3 mgL^{-1}, and the pH at 5 for a reaction duration of 80 minutes. The degradation (%) of the D.R. 31 dye solution in the U.V. irradiation system was evaluated, as shown in Figure 10c, at various H_2O_2 concentrations ranging from 0.01 mM to 0.05 mM. Figure 10c shows that the photodegradation efficiency of D.R. 31 dye increases somewhat up to 60.74 % by increasing the concentration of H_2O_2 from 0.01 to 0.03 mM (optimal dose) with the addition of H_2O_2. Given that the H_2O_2 concentration is closely correlated with the quantity of OH• radicals produced during the photo-assisted catalytic process, this result suggests that the H_2O_2 content may be crucial in increasing the degradation percentage of D.R. 31 dye (Harun *et al.* 2020). A similar observation for the use of H2O2 as a photocatalyst in the degradation of other organic pollutants has been documented in the literature previously (Chen and Liu, 2007). When the H_2O_2 concentration rises from 0.03 mM to 0.05 mM, the photodegradation efficiency does, however, decrease. The results are consistent with the literature (Zha *et al.* 2022). At increasing H_2O_2 concentrations, the surplus H_2O_2 molecules scavenge the beneficial • O.H. produced by the direct photolysis of H_2O_2 and form a much weaker oxidant of HO•2 (Equation 1) (Chen and Liu, 2007). Furthermore, increased H2O2 concentrations may absorb and lessen incident U.V. radiation that is needed for photocatalysis (Halbus *et al.* 2013). As a result, the system's overall oxidation capacities are decreased (equation 2), and the following equations show the deceleration of the deterioration rates:

$$H_2O_2 + \bullet OH \rightarrow HO_2\bullet + H_2O \quad (1)$$

$$HO_2\bullet + \bullet OH \rightarrow H_2O + O_2 \quad (2)$$

As a result, in the current study, the optimal concentration of H_2O_2 for photocatalytic decomposition of D.R. 31 dye under U.V. irradiation is 0.03 mM. Equation (3) indicates that when a potent peroxide agent, like hydrogen peroxide (H_2O_2), is present, the photolysis process might increase the generation of • O.H. At greater concentrations, H_2O_2 is known to prevent electron-hole recombination in addition to producing hydroxyl radicals when an electron is abstracted from the conduction band (Ruiz-López *et al.* 2021).

$$H_2O_2 + hv(<385nm) \rightarrow 2\bullet OH \quad (3)$$

3.3.4 Effect of different pH levels on Photo-degradation

In the study of photo-catalysis, pH is one of the most important parameters regulating the rate of decomposition of particular organic molecules. It is also a critical operational variable in wastewater treatment (Moradi and Ganjali, 2019). The D.R. 31 dye degradation was studied at different pH values ranging from 5 to 10. Low pH decolorization was effective, and the rate constant was in the order of 5>6>7>8>9>10. Plotting of the degradation (%) at different pH levels is shown in Figure 10d. It has been noted that D.R. 31's photodegradation effectiveness is enhanced by an acidic pH. D.R. 31 has a pH of about eight by nature. Dhas *et al.* (2015) stated that the acidic nature of the dye solution causes the increased rate of ionization of two sulfuric groups, and more dye anions could be adsorbed on the catalyst surface due to electrostatic attraction. Thus, the D.R. anion's positive surface charge could be readily oxidized to O^{2-} present in the Co_3O_4/Na-Alg NC catalyst surface. Though the $^{-}$O.H. ion radical is unstable at higher pH values, the decreased production of this radical may be the cause of the poor photo-degradation seen in alkaline media (Dhas *et al.* 2015; Rahmat *et al.* 2023).

3.3.5 Effect of different temperature levels on Photo-degradation

Similarly, it was also studied how temperature affected the percentage of D.R. 31 dye decolorization using Co_3O_4/Na-Alg NC as a photocatalyst. The temperature effect on the decolorization of D.R. 31 was calculated at 40–80°C by taking other parameters with their optimal values as dye concentration 0.02 %, catalyst concentration 3mgL^{-1} and pH 5. The experiments were left to run for 80 min. As shown in Figure 10e, the percentage of dye decolorization increased up to 68.24% at 70°C (optimal value) with a temperature increase from 40 to 70°C. Generally, increasing the temperature can increase the kinetic energy of molecules, including the dye molecules and the adsorbent surface. This higher kinetic energy may cause the dye molecules and the adsorbent surface to clash more strongly, initially enhancing the adsorption capacity.

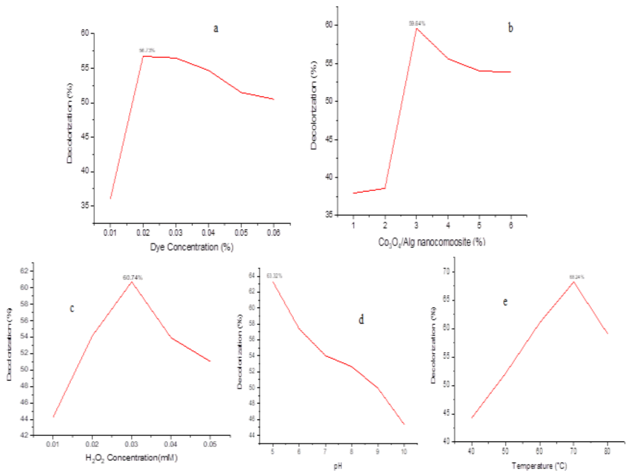

Figure 11. Effect of (a) dye concentration (b) Co_3O_4/Na-Alg nanocomposite level (c) H2O2 dose (d) pH (e) different levels of temperature on decolorization of Direct Red 31 dye using Co_3O_4/Na-Alg Nanocomposites as a catalyst

Temperature-related changes in the physical properties of the adsorbent material, such as variations in porosity or surface area, may also have an effect on adsorption capacity. When subjected to temperatures over their optimal level, catalyst efficiency may be reduced. Higher temperatures reduce the adsorption capacity of Co_3O_4/Na-Alg NC (Kiran *et al.* 2021; Rafique *et al.* 2023), which is likely due to the sintering and temperature increase procedure. That results in a reduction in the surface area of the catalyst for alteration in the catalyst's three-dimensional shape, which may hinder the active binding of substrate, resulting in a decrease in reaction rate (Khalil *et al.* 2021). It could be because the sintering process at higher temperatures reduces the catalytic surface, reducing the catalyst's ability to adsorb chemicals (Mohammad *et al.* 2016; Kishore *et al.* 2023). Moreover, at higher temperatures, competitive reactions like desorption or disintegration of adsorbed molecules may occur. Approaching equilibrium may lead to a decline in the system's total adsorption capacity (Jaina *et al.* 2023).

3.4 Kinetics study

The decolorization of dye is studied kinetically by applying a linear data-fitting model. Dye degradation by Co_3O_4/Na-Alg Nanocomposites catalyst is studied kinetically with respect to time. The experimental data for D.R. 31 dye is obtained from the spectrometric analysis, and data is treated to find the order of the Dye degradation reaction. It is observed from Figure 11a that data is plotted between dye concentration and time for dye decolorization. It is clearly observed that data for D.R. 31 dye decolorization does not follow a zero-order reaction. Then, data is plotted between ln[dye] and degradation time, as shown in Figure 11b, using spectrometer data to study the 1st-order reaction kinetics. Furthermore, the graph is plotted between ln1/[dye] and time for study second order kinetics using Co_3O_4/Na-Alg nanocomposites. The slope R^2 values for zero, first and second order are measured as 0.9663, 0.9897 and 0.9815, respectively. The R^2 value is found to be highest for 1st order reaction. Figure 11b represents R^{2}'s highest value for first order exhibited that dye decolorization reaction follows first order reaction kinetics. First-order kinetics depicts an instance where the degree of dye degradation through nanocomposite is proportional to the dye concentration at any given moment. This suggests that the dye's rate of degradation will fall proportionally as its level does (Haritha *et al.* 2016; Fardood *et al.* 2019).

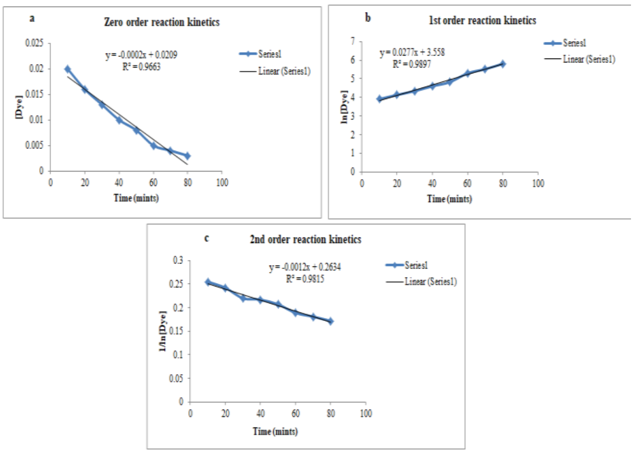

Figure 11. Kinetic of D.R. 31 dye degradation reaction using Co_3O_4/Na-Alg nanocomposites

3.5 Mineralization Study

Both C.O.D. and T.O.C. tests are used to monitor the efficiency of wastewater treatment processes. By measuring the organic load before and after treatment, operators can evaluate how well the treatment process is removing organic pollutants. The mineralization efficiency of D.R. 31 dye samples treated with Co_3O_4/Na-Alg nanocomposites as a catalyst was determined by analyzing quality assurance parameters for water, such as C.O.D. and T.O.C. C.O.D. and T.O.C. measurements were performed on the treated D.R. 31 dye solution. It indicated a gradual improvement in mineralization with a rise in reaction time and a gradual increase in elimination

(%) of both C.O.D. and T.O.C. The percentage reduction (%) in C.O.D. and T.O.C. after catalytic treatment was 66.7% and 65.2%, respectively (Figure 12). Thus, it can be concluded that Co_3O_4/Na-Alg nanocomposites ensure the degradation of the targeted dye by reducing the C.O.D. and T.O.C. of the solution in addition to removing the dye. The current study's findings are consistent with previous research (Islam *et al.* 2019; Ahmed *et al.* 2022).

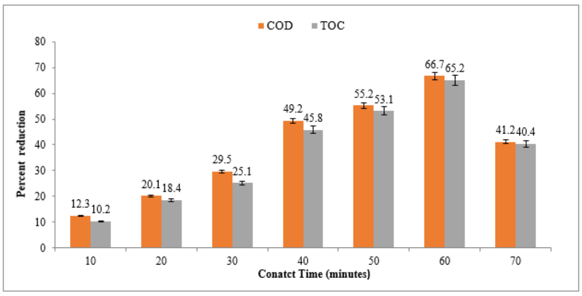

Figure 12. Effect of catalytic process contact time on per cent reduction of chemical oxygen demand (C.O.D.) and total organic carbon (T.O.C.)

3.6 Photocatalytic pathway for degradation of Direct Red 31 dye

Electrons are excited and migrate to the catalyst conduction band when light with an energy equal to or greater than the photo catalyst's (Co_3O_4/Na-Alg NC) band gap energy shines on it. As a result, holes in the valance band (V.B.) and electrons in the conduction band (C.B.) are created, which initiate the photo-degradation process of DR31 dye by taking part in redox reactions (Koli *et al.* 2018). Strong oxidants such as hydroxyl radicals (• O.H.) help destroy dye. It is created by a number of processes, such as the breakdown of hydrogen peroxide and the interaction of photo-generated holes with hydroxide anion and water molecules. Degradation of dyes can occur quickly due to the potent and non-selective oxidative power of hydroxyl radicals. The chemical processes lead to dye degradation, as discussed in Figure 13.

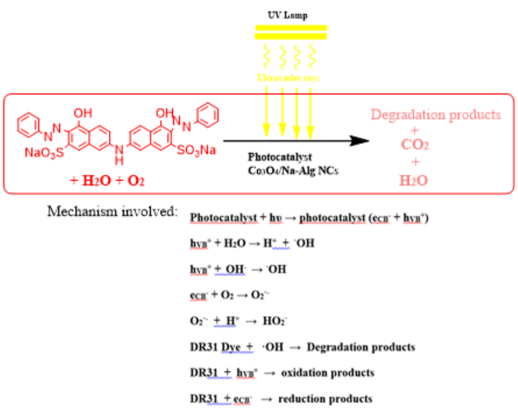

Figure 13. Photo-degradation pathway of Direct Red 31 dye

Photo-generated pairs combine and release the stored energy instantaneously when no electron scavengers are present. Materials such as molecular oxygen stop electron and hole recombination. Oxygen is one of the electron acceptors that photo-generated electrons can react with to produce the superoxide anion radical (Tahir and Saad, 2021). The Co_3O_4/Na-Alg NC was employed as a photocatalyst for the first time; the D.R. 31 dye was successfully decomposed by following the mechanism explained in Figure 13. The Co_3O_4/Na-Alg NC photocatalyst shows efficient degradation like other nanocomposites of cobalt oxide (Bankole *et al.* 2020; Mohamed *et al.* 2022).

4. Conclusion

The first time ever prepared the Co_3O_4/Na-Alg nanocomposites demonstrated to be successful in textile wastewater treatment. The synthesis of Co_3O_4/Na-Alg nanocomposites was carried out using a chemical method. Optical (U.V.–Visible), S.E.M. (morphological), structural (X-ray diffraction), and elemental (FTIR) methods were used to characterize the produced Co_3O_4 nanoparticles (Co_3O_4 NPs) and Co_3O_4/sodium alginate nanocomposite (Co_3O_4/Na-Alg NC). Dyes can be efficiently destroyed by photocatalysis in the presence of Co_3O_4/Na-Alg nanocomposites. Co_3O_4/Na-Alg NCs' photo-catalytic behaviour has been evaluated in an aqueous phase using D.R. 31 dye, guaranteeing a degradation efficiency of about 67.24% under visible light. The activities of Co_3O_4/Na-Alg photocatalysts are influenced by a number of operating parameters. Using three mg/L conc. Of Co_3O_4/Na-Alg NC produced the greatest photo degradation efficiency. Under U.V. irradiation, the values of D.R. 31 degrading with Co_3O_4/Na-Alg nanocomposites were measured to be 67.24%. The maximum degradation was achieved at 0.02% dye concentration and three mg/L concentration of Co_3O_4/Na-Alg NC, 0.03mM H_2O_2, pH 5, 70°C during 80 minutes of reaction. The percentage reduction in C.O.D. and T.O.C. was 65.2% and 66.7%, respectively, which has shown the effectiveness of the current method of study.

Acknowledgments

The authors are grateful to the Department of Applied Chemistry at Government College University in Faisalabad, Pakistan, for providing the essential research facilities for this study. This study is carried out under the supervision of Dr. Shumaila Kiran, Associate Professor, Department of Applied Chemistry, Government College University Faisalabad, Pakistan. This research study belongs to the part of the Ph.D thesis of Ms Saba Naz.

Author contributions

S.N.: doing experimental work and writing original drafts; SK: conceptualization, supervision, draft checking; TG-technical evaluation, data interpretation; T.F.: review and editing. All authors read and approved the final manuscript.

Funding

Not applicable.

Availability of data and materials

All data analyzed during this research work is presented in this article.

Declarations

Not applicable.

Ethics approval consent to participate

Consent for publication

Not applicable.

Competing interests

The authors declare no competing interests.

References

Abd El-Aziz H.M., Zayed, M.A. and Abdel-Gawad, S.A. (2024). Adsorptive removal of Direct Red 31 and Direct Orange 26 azo dyes from aqueous solutions using Ficus nano zero valent copper: Linear, non-linear, response surface methodology (R.S.M.), and artificial neural network (ANN) modelling. *Adsorption Science & Technology*, **42**, 1–24. https://doi.org/10.1177/0263617424125.

Ahmed F., Gulzar T., Kiran S., Ahmad I., Fatima A., Yasir S. and Kamal T. (2022). Nickel oxide and carboxymethyl cellulose composite beads as catalysts for pollutant degradation. *Applied Nanoscience,* **12**(11), 3585–3595. https://doi.org/10.1007/s13204-022-02345-5.

Akhter P., Nawaz S., Shafiq I., Nazir A., Shafique S., Jamil F. and Hussain M. (2023). Efficient visible light-assisted photocatalysis using ZnO/TiO_2 nanocomposites. *Molecular Catalysis,* **535**, 112896. https://doi.org/10.1016/j.mcat.2022.112896.

Akram M., Gao B., Pan J., Khan R., Inam M.A., Xu X. and Yue Q. (2022). Enhanced removal of phosphate using pomegranate peel-modified nickel-lanthanum hydroxide. *Science of The Total Environment*, **809**, 151181.

Akram M., Bhutto S.U.A., Aftab S., Sindhu L., Xu X. and Haider Z. (2023). Nanocomposites for removal and degradation of organic pollutants. In *Modern Nanotechnology: **1**: Environmental Sustainability and Remediation*, 519–558. Springer International Publishing.

Akram M., Bano Z., Bhutto S.U.A., Pan J., Uddin A., Afzal M.Z. and Wang F. (2024). Highly efficient nickel recovery from industrial wastewater via synergistic electrodeposition and electrocatalytic oxidation technique. *Journal of Environmental Chemical Engineering*, **12**(3), 112830.

Al-Askar A.A., Hashem A.H., Elhussieny N.I. and Saied, E. (2023). Green Biosynthesis of Zinc Oxide Nanoparticles Using *Pluchea indica* Leaf Extract: Antimicrobial and Photocatalytic Activities. *Molecules,* **28**(12), 4679. https://doi.org/10.3390/molecules28124679.

Alavinia S. Ghorbani-Vaghei R. Asadabadi S. and Atrian A. (2023). Sodium alginate/diethyleneamine-triazine-sulfonamide nanocomposite for adsorptive removal of Pb (II) and methyl violet from aqueous solutions. *Materials Chemistry and Physics,* **293**, 126915. https://doi.org/10.1016/j.matchemphys.2022.126915.

Al-Enizi A.M., Karim A. and Yousef A. (2023). A novel method for fabrication of electrospun cadmium sulfide nanoparticles-decorated zinc oxide nanofibers as effective photocatalyst for water photosplitting. *Alexandria Engineering Journal,* **65**(2), 825–835. https://doi.org/10.1016/j.aej.2022.09.049.

Attia Y.A. and Abdel-Hafez S.H. (2021). Nano-Co_3O_4-catalyzed microwave-assisted one-pot synthesis of some seleno [2, 3-b] pyridine/quinoline derivatives. *Research on Chemical Intermediates,* **47**(9), 3719–3732.

Bankole O.M., Olaseni S.E., Adeyemo M.A. and Ogunlaja A.S. (2020). Microwave-assisted synthesis of cobalt oxide/reduced graphene oxide (Co_3O_4–rGo) composite and its sulfite enhanced photocatalytic degradation of organic Dyes. *Zeitschrift für Physikalische Chemie*, **234**(10), 1681–1708.

Bano Z., Akram M., Ali N.Z., Khan M.U., Wang F., Li L. and Xia M. (2024). Sustainable porous graphene/Co-MOF for the removal of water pollutants: Combined theoretical and experimental studies. *Journal of Water Process Engineering*, **59**, 104982.

Bhargava R., Khan S., Ahmad N. and Ansari M.M.N. (2018). Investigation of structural, optical and electrical properties of Co_3O_4 nanoparticles. In: *A.I.P. conference proceedings*, **1953**, No. 1. A.I.P. Publishing. https://doi.org/10.1063/1.5032369.

Bhutto S.U.A., Akram M. and You X.Y. (2024). Probabilistic risk assessment of microplastics in Tai Lake, China. *Science of The Total Environment*, **914**, 169965.

Chang N., Chen Y.R., Xie F., Liu Y.P. and Wang H.T. (2020). A promising Z-scheme heterojunction via loading Ag/AgCl into porous Co_3O_4 derived from ZIF-67 for visible light-driven photocatalysis. *Microporous and Mesoporous Materials,* **307**(11), 110530–110541. https://doi.org/10.1016/j.micromeso.2020.110530.

Chen S. and Liu Y. (2007). Study on the photocatalytic degradation of glyphosate by TiO_2 photocatalyst. *Chemosphere,* **67**(5), 1010–1017. https://doi.org/10.1016/j.chemosphere.2006.10.054.

Dammala P., Machado J., Rani B., Murali S., Devi S., Luwang M.N. and Sahu N.K. (2019). Synthesis of biphasic nanomaterials based on ZnO and SnO_2: Application towards photocatalytic degradation of acid red dye. *Nano-Structures and Nano-Objects,* **18**(4), 292–301. https://doi.org/10.1016/j.nanoso.2019.100292.

Dhas C.R., Venkatesh R., Jothivenkatachalam K., Nithya A., Benjamin B.S., Raj A.M.E. and Sanjeeviraja C. (2015). Visible light-driven photocatalytic degradation of Rhodamine B and Direct Red using cobalt oxide nanoparticles. *Ceramics Internationals,* **41**(8), 9301–9313. https://doi.org/10.1016/j.ceramint.2015.03.238.

Elashery S.E., Ibrahim I., Gomaa H., El-Bouraie M.M., Moneam I.A., Fekry S.S. and Mohamed G.G. (2023). Comparative study of the photocatalytic degradation of crystal violet using ferromagnetic magnesium oxide nanoparticles and MgO-bentonite nanocomposite. Magnetochemistry, 9(2), 56. https://doi.org/10.3390/magnetochemistry9020056.

Elsharawy A.I., Yakout S.M., Wahba M.A., Abdel-Shafi A.A. and Khalil M.S. (2023). Transition-metal blends incorporated into CuO nanostructures: Tuning of room temperature spin-ferromagnetic order. *Solid State Sciences,* **139**(5), 107166. https://doi.org/10.1016/j.solidstatesciences.2023.107166.

Eskikaya O., Isik Z., Arslantas C., Yabalak E., Balakrishnan D., Dizge N. and Rao K.S. (2023). Preparation of hydrochar bio-based catalyst for Fenton process in dye-containing wastewater treatment. *Environmental Research,* **216**(1), 114357. https://doi.org/10.1016/j.envres.2022.114357.

Fan X., Xu Y., Ma C. and He W. (2021). In-situ growth of Co_3O_4 nanoparticles based on electrospray for an acetone gas sensor. *Journal of Alloys and Compounds,* **854** 157234. https://doi.org/10.1016/j.jallcom.2020.157234.

Fardood T.S., Moradnia F. and Ramazani A. (2019). Green synthesis and characterization of ZnMn2O4 nanoparticles for photocatalytic degradation of Congo red dye and kinetic study. *Micro and Nano Letters,* **14**(9), 986–991.

Farhadi S., Javanmard M. and Nadri G. (2016). Characterization of cobalt oxide nanoparticles prepared by the thermal decomposition. *Acta Chimica Slovenica,* **63**(2), 335–343.

Ghaffar A., Kiran S., Rafique, M.A., Iqbal, S., Nosheen, S., Hou, Y. and Aimun, U. (2021). *Citrus paradisi* fruit peel extract mediated green synthesis of copper nanoparticles for remediation of dispersed yellow 125 dye. *Desalination and Water Treatment,* **212**(7), 368–375. https://doi.org/10.5004/dwt.2021.26684.

Ghobadifard M., Foroomand S. and Mohebbi S. (2023). Photocatalytic conversion of M.B. dye using Co_3O_4 QDs-Ag_2MoO_4 as an active heterojunction photocatalyst under visible light irradiation. *Applied Organometallic Chemistry,* **37**(6), 7071. https://doi.org/10.1002/aoc.7071.

Gola D., Bhatt N., Bajpai M., Singh A., Arya A., Chauhan N., Srivastava S.K., Tyagi P.K. and Agrawal, Y. (2021). Silver nanoparticles for enhanced dye degradation. *Current Research in Green and Sustainable Chemistry*, **4**, 100132. https://doi.org/10.1016/j.crgsc.2021.100132.

Greenberg A.E., Trussell R.L. and Clesceri, L.S. (1985). Standard Methods for the Examination of Water and Wastewater. 20th Ed., American Public Health Association, Washington, DC, 38.

Hadadi A., Imessaoudene A., Bollinger J.C., Bouzaza A., Amrane A., Tahraoui H. and Mouni L. (2023). Aleppo pine seeds (*Pinus halepensis Mill.)* as a promising novel green coagulant for the removal of Congo red dye: Optimization via a machine learning algorithm. *Journal of Environmental Management,* **331**(4), 117286. https://doi.org/10.1016/j.jenvman.2023.117286.

Hai Z., Gao L., Zhang Q., Xu H., Cui D., Zhang Z. and Xue, C. (2016). Facile synthesis of core-shell structured PANI-Co3O4 nanocomposites with superior electrochemical performance in supercapacitors. *Application of Surface Science,* **361**, 57–62.

Halbus A.F., Athab Z.H. and Hussein F.H. (2013). Adsorption of dispersed blue dye on Iraqi date palm seeds activated carbon. *International Journal of Chemical Science,* **11**(3), 1219–1233. https://doi.org/abstract/20143005010.

Haritha E., Roopan S.M., Madhavi G., Elango G., Al-Dhabi N.A. and Arasu M.V. (2016). Green chemical approach towards the synthesis of SnO_2 NPs in an argument with photocatalytic degradation of diazo dye and its kinetic studies. *Journal of Photochemistry Photobiology B: Biology* **162**, 441–447.

Harun N., Sheng C.K., Sabri M.G.M., Dagang A.N. and Salleh, H. (2020). Impact of TiO_2 and H_2O_2 on photocatalytic degradation of phodamine B under ultraviolet c (uv-c) radiation for efficient polluted wastewater treatment. *Journal of Optoelectronic and Biomedical Materials,* **12**(1) 9–15 (2020). https://doi.org/10.15251/JOBM.2020.121.9.

Hecht H. and Srebnik S. (2016). Structural characterization of sodium alginate and calcium alginate. Biomacromolecules, 17(6), 2160–2167. https://doi.org/10.1021/acs.biomac.6b00378.

Helmiyati H. and Wahyuningrum K.D. (2018). Synthesis and photocatalytic activity of nanocomposite based on sodium alginate from brown algae with ZnO impregnation. In: *A.I.P. Conference Proceedings*, Vol. 2023, No. 1. A.I.P. Publishing L.L.C. https://doi.org/10.1063/1.5064104.

Hu P., Meng C., Cai Y., Wang P., Zhou H., Li X. and Yuan A. (2023). Supernano crystals boost the initial coulombic efficiency and capacity of copper benzene-1, 3, 5-tricarboxylate for Li-Ion batteries. Energy Fuels, **37**(4), 34–41. https://doi.org/10.1021/acs.energyfuels.2c03125.

Islam S., Shaikh I.A., Firdous N., Ali A. and Sadef Y. (2019). A new approach for the removal of unfixed dyes from reactive dyed cotton by Fenton oxidation. *Jounal of Water Reuse and* Desalination, **9**(2) 133–141. https://doi.org/10.2166/wrd.2019.011.

Jaina S., Bhatt A., Baba S.A., Bisht V.S., Biswas P., Ambatipudi K. and Navani N.K. (2023). Concurrent mitigation and facile monitoring of xenobiotics by a highly efficient and recyclable nanoengineered catalyst. *Chemical Engineering Journal,* **89** 145074. https://doi.org/10.1016/j.cej.2023.145074.

Karim M.A.H., Aziz, K.H.H., Omer, K.M., Salih, Y.M., Mustafa, F., Rahman, K.O. and Mohammad, Y. (2021). Degradation of aqueous organic dye pollutants by heterogeneous photo-assisted Fenton-like process using natural mineral activator: Parameter optimization and degradation kinetics. In: *I.O.P. Conference Series: Earth and Environmental Science,* **958**, No. 1, 012011, I.O.P. Publishing. https://doi.org/10.1088/1755-1315/958/1/012011.

Khalaji A.D. (2019). Synthesis, characterization and optical properties of Co_3O_4 nanoparticles. *Asian Journal of Nanoscience and Materials,* **2**(2), 186–190. https://doi.org/10.26655/ajnanomat.2019.3.5.

Khalil A., Ali N., Asiri A.M., Kamal T., Khan S.B. and Ali J. (2021). Synthesis and catalytic evaluation of silver nickel oxide and alginate biopolymer nanocomposite hydrogel beads. *Cellulose,* **28**, 11299–11313. https://doi.org/10.1007/s10570-021-04248-0.

Kharat S.D., Pondkule S.A., Dongare R.K., Patole S., Karpoormath R., Inamdar S. and Shinde M.P. (2023). Catalytic applications of cobalt/cobalt oxide nanoparticles in heterocyclic compounds. *Materials Today: Proceedings.* https://doi.org/10.1016/j.matpr.2023.06.178.

Kiran S. Rafique M.A., Ashraf A., Farooq T., Iqbal S., Afzal G. and Naz S. (2021). Green synthesis of nickel nanoparticles using fruit peels of *Citrus Paradise* for remediation of Congo red dye. *Journal of Mexican Chemical Society,* **65**(4), 507–515. https://doi.org/10.29356/jmcs.v65i4.1572.

Kiran S., Rafique M.A., Iqbal S., Nosheen S., Naz, S. and Rasheed A. (2020). Synthesis of nickel nanoparticles using *Citrullus colocynthis* stem extract for remediation of Reactive Yellow 160 dye. *Environmental Science and Pollution Research,* **27**(26), 32998–33007. https://doi.org/10.1007/s11356-020-09510-9.

Kiran S., Adeel S., Nosheen S., Hassan A., Usman M. and Rafique M.A. (2017). Recent trends in textile effluent treatments: A review. *Advances in Materials and Wastewater Treatment,* 29–49. https://doi.org/10.1002/9781119407805.

Kiran S., Nosheen S., Iqbal S., Abrar S., Jalal F., Gulzar T. and Naseer N. (2018). Photocatalysis using titanium dioxide for treatment of textile wastewater containing disperse dyes. *Chiang Mai Journal of Science,* **45**, 2730–2739. https://doi.org/10.Article/CMJS/10990421.

Kishore, K., Hsu, C. Y., Sridhara, S., Odongo, J. O., Akram, M., Malik, J. A., ... & Manzoor, J. (2023). Fundamentals of Nanotechnology for Environmental Engineering. In *Modern Nanotechnology: Volume 1: Environmental Sustainability and Remediation*, 1-19, Springer International Publishing.

Koli P.B., Kapadnis K.H., Deshpande U.G. and Patil M.R. (2018). Fabrication and characterization of pure and modified Co_3O_4 nanocatalyst and their application for photocatalytic degradation of eosine blue dye: a comparative study. *Journal of Nanostructures Chemistry*, **8**, 453–463. https://doi.org/10.1007/s40097-018-0287-0.

Krishnan A., Swarnalal A., Das D., Krishnan M., Saji V.S. and Shibli S.M.A. (2024). A review on transition metal oxides based photocatalysts for degradation of synthetic organic pollutants. *Journal of Environmental Science,* **139**(5), 389–417. https://doi.org/10.1016/j.jes.2023.02.051

Kumar N., Pandey A. and Sharma Y.C. (2023). A review on sustainable mesoporous activated carbon as adsorbent for efficient removal of hazardous dyes from industrial wastewater. *Journal of Water Process Engineeribg,* **54,** 104054. https://doi.org/10.1016/j.jwpe.2023.104054.

Kumarage G.W. and Comini E. (2021). Low-dimensional nanostructures based on cobalt oxide (Co_3O_4) in chemical-gas sensing. *Chemosensors,* **9**(8), 197. https://doi.org/10.3390/chemosensors9080197.

Lakra R. Kumar R. Thatoi D.N. Sahoo P.K. and Soam A. (2021). Synthesis and characterization of cobalt oxide (Co_3O_4) nanoparticles. *Materials Today Proceedings,* **41**, 269–271. https://doi.org/10.1016/j.matpr.2020.09.099.

Lanzetta A., Papirio S., Oliva A., Cesaro A., Pucci L., Capasso E.M. and Pirozzi F. (2023). Ozonation processes for color removal from urban and leather tanning wastewater. *Water,* **15**(13), 2362. https://doi.org/10.3390/w15132362.

Lin Q., Ding J., Yang Y., Sun F., Shen C., Lin H. and Su X. (2023). Simultaneous adsorption and biodegradation of polychlorinated biphenyls using resuscitated strain *Streptococcus sp.* SPC0 immobilized in polyvinyl alcohol-sodium alginate. *Science of the Total Environment,* **868**, 161620. https://doi.org/10.1016/j.scitotenv.2023.161620.

Mahdiani M., Soofiv F., Ansari F. and Salavati-Niasari M. (2018). Grafting of $CuFe_{12}O_{19}$ nanoparticles on C.N.T. and graphene: Ecofriendly synthesis, characterization and photocatalytic activity. *Journal of Cleaner Production,* **176**(3), 1185–1197. https://doi.org/10.1016/j.jclepro.2017.11.177.

Maniammal K., Madhu G. and Biju V. (2018). Nanostructured mesoporous NiO as an efficient photocatalyst for degradation of methylene blue: Structure, properties and performance. *Nano-Structures and Nano-Objects,* **16**(10), 266–275. https://doi.org/10.1016/j.nanoso.2018.07.007.

Matei D., Katsina A.U., Mihai S., Cursaru D.L., Şomoghi R. and Nistor C.L. (2023). Synthesis of Ruthenium-Promoted ZnO/SBA-15 Composites for Enhanced Photocatalytic Degradation of Methylene Blue Dye. *Polymers,* **15**(5), 1210–1220. https://doi.org/10.3390/polym15051210.

Mayakkannan M., Siva V., Murugan A., Shameem A., Thangarasu S. and Bahadur S.A. (2023). Microwave-assisted synthesis of ternary transition metal ferrite: Structural, morphological, optical, magnetic and electrochemical properties. *Physica E: Low-Dimensional System and Nanostructures,* **147**(3), 115573.

Mohamed R.M., Ismail, A.A., Basaleh, A.S., and Bawazir, H.A. (2022). Ease synthesis of porous Copper oxide/Cobalt oxide heterostructures for superior photodegradation of Foron Blue dye. *Optical Materials*, 124, 112000.

Mohammad E.J., Lafta A.J. and Kahdim S.H. (2016). Photocatalytic removal of reactive yellow 145 dye from simulated textile wastewaters over supported (Co, $Ni)_3O_4/Al_2O_3$ co-catalyst. *Polish Journal of Chemical and Technology,* **18**(3),1–9. https://doi.org/10.1515/pjct-2016-0041.

Moradi R. and Ganjali A. (2019). Synthesis of Fe_3O_4 Nanoparticles and Their Application in Photo-Fenton Degradation of Direct Red 23 Dye in Aqueous Solutions. *Russian Journal of Physical Chemistry A,* **93**(1), 2789–2797. https://doi.org/10.1134/S0036024419130211.

Nastaj J., Przewłocka A. and Rajkowska-Myśliwiec M. (2016). Biosorption of Ni (II), Pb (II) and Zn (II) on calcium alginate beads: equilibrium, kinetic and mechanism studies. *Polish Journal of Chemical and Technology,* **18**(3), 81–87. https://doi.org/10.1515/pjct-2016-0052.

Negash A., Tibebe D., Mulugeta M. and Kassa Y. (2023). A study of basic and reactive dyes removal from synthetic and industrial wastewater by electrocoagulation process. *South African Journal of Chemical Engineering,* **46**(10) 122–131. https://doi.org/10.1016/j.sajce.2023.07.015.

Obisesan O.R., Adekunle A.S., Oyekunle J.A.O., Sabu T., Nkambule T.T.I. and Mamba B.B. (2019). Development of electrochemical nanosensor for the detection of malaria parasite in clinical samples. *Frontiers in Chemistry,* **7**(2), 89–104. https://doi.org/10.3389/fchem.2019.00089.

Patra T., Mohanty A., Singh L., Muduli S., Parhi P.K. and Sahoo T.R. (2022). Effect of calcination temperature on morphology and phase transformation of MnO_2 nanoparticles: A step towards green synthesis for reactive dye adsorption. *Chemosphere*, **288**, 64–72. https://doi.org/10.1016/j.chemosphere.2021.132472.

Rafique M.A., Kiran S., Jamal A., Abrar S., Jalal F. and Rahman N. (2023). Nickel nanoparticles synthesized from *Psidium guajava* peels mediated degradation of Orange E_3 dye reactive dye: a sustainable approach. *International Journal of Environmental Science and Technology,* **20**(3), 2733–2744. https://doi.org//10.1007/s13762-022-04509-w.

Rahmat M., Kiran S., Gulzar T., Yusuf M., Nawaz R., Khalid J. and Azam M. (2023). Plant-assisted synthesis and characterization of MnO_2 nanoparticles for removal of crystal violet dye: an environmental remedial approach. *Environmental Science and Pollution Research,* **30**(20), 57587–57598.

Raji F., Zafari M., Rahbar-Kelishami A. and Ashrafizadeh S.N. (2023). Enhanced removal of methyl orange using modified anion exchange membrane adsorbent. *International Journal of Environmental Science and Technology,* **20**(7), 9823–9836. https://doi.org/10.1007/s13762-023-05089-z.

Roy H., Rahman T.U., Khan M.A.J.R., Al-Mamun M.R., Islam S.Z., Khaleque M.A. and Awual M.R. (2023). Toxic dye removal, remediation, and mechanism with doped SnO_2-based nanocomposite photocatalysts: A critical review. *Journal of Water Process Engineering,* **54**(8), 104069. https://doi.org/10.1016/j.jwpe.2023.104069.

Ruiz-Lopez M.F., Martins-Costa M.T., Francisco J.S. and Anglada J.M. (2021). Tight electrostatic regulation of the O.H.

production rate from the photolysis of hydrogen peroxide adsorbed on surfaces. *Proceedings of the National Academy Sciences,* **118**(30), 2106117118. https://doi.org/10.1073/pnas.2106117118.

Samer M., Abdelsalam E.M., Mohamed S., Elsayed H. and Attia Y. (2022). Impact of photoactivated cobalt oxide nanoparticles addition on manure and whey for biogas production through dry anaerobic co-digestion. *Environmental Development and Sustainability,* **24**(6), 7776–7793. https://doi.org/10.1007/s10668-021-01757-7.

Sellimi S., Younes I., Ayed H.B., Maalej H., Montero V., Rinaudo M. and Nasri M. (2015). Structural, physicochemical and antioxidant properties of sodium alginate isolated from a Tunisian brown seaweed. *International Journal of Biological Macromolecules,* **72**(1), 1358–1367. https://doi.org/10.1016/j.ijbiomac.2014.10.016.

Sheikh M.S., Rahman M.M., Rahman M.S., Yildirim K. and Maniruzzaman M. (2023). Fabrication of nano composite membrane filter from graphene oxide (G.O.) and banana rachis cellulose nano crystal (C.N.C.) for industrial effluent treatment. *Journal of Industrial and Engineering Chemistry,* https://doi.org/10.1016/j.jiec.2023.07.048.

Shen L. and Wang C. (2014). Hierarchical Co_3O_4 nanoparticles embedded in a carbon matrix for lithium-ion battery anode materials. *Electrochim. Acta* **133**, 16–22. https://doi.org/10.1016/j.electacta.2014.03.182.

Shokoohi R., Salari M., Safari R., Zolghadr Nasab H. and Shanehsaz S. (2021). Modelling and optimisation of catalytic ozonation process assisted by ZrO_2-pumice/H_2O_2 in the degradation of Rhodamine B dye from aqueous environment. *International Journal of Environmental and Analytical Chemistry,* **101**(15), 2629–2653. https://doi.org/10.1080/03067319.2019.1704748.

Steel R.G., Torrie J. and Dickey D.A. (1997). Principles and Procedures of Statistics. A Biochemical Approaches. McGraw Hill, Inc. Book Co., New York, U.S.A.

Sujatha K., Seethalakshmi T., Sudha A.P. and Shanmugasundaram O.L. (2019). Photocatalytic activity of pure, Zn doped and surfactants assisted Zn doped SnO_2 nanoparticles for degradation of cationic dye. *Nano-Structures and Nano-Objects,* **18**(4), 305–315. https://doi.org/10.1016/j.nanoso.2019.100305.

Tahir H. and Saad M. (2021). Using dyes to evaluate the photocatalytic activity. In: *Interface Science and Technology,* **32**, 125–224. Elsevier. https://doi.org/10.1016/B978-0-12-818806-4.00005-X.

Tai V.C., Che H.X., Kong X.Y., Ho K.C. and Ng W.M. (2023). Decoding iron oxide nanoparticles from design and development to real world application in water remediation. *Journal of Industrial and Engineering Chemistry,* **127**(11), 82–100. https://doi.org/10.1016/j.jiec.2023.07.038.

Tyagi A., Banerjee S., Cherusseri J. and Kar K.K. (2020). Characteristics of transition metal oxides. *Handbook of Nanocomposite Supercapacitor Materials I: Characteristics*. **300**(4), 91–123. https://doi.org/10.1007/978-3-030-43009-2_3.

Vinayagam R., Hebbar A., Kumar P.S., Rangasamy G., Varadavenkatesan T., Murugesan G. and Selvaraj R. (2023). Green synthesized cobalt oxide nanoparticles with photocatalytic activity towards dye removal. *Environmental Research,* **216**(4), 114766. https://doi.org/10.1016/j.envres.2022.114766.

Waliullah R.M., Rehan A.I., Awual M.E., Rasee A.I., Sheikh M.C., Salman M.S. and Awual M.R. (2023). Optimization of toxic dye removal from contaminated water using chitosan-grafted novel nanocomposite adsorbent. *Journal of Molecular Liquids,* **388**(10), 122763. https://doi.org/10.1016/j.molliq.2023.122763.

Wu K.H., Jiang Y., Jiao S., Chou K.C. and Zhang G.H. (2020). Synthesis of high purity nano-sized transition-metal carbides. *Journal of Material Research Technology,* **9**(5), 778–790. https://doi.org/10.1016/j.jmrt.2020.08.053.

Xu H., Hai Z., Diwu J., Zhang Q., Gao L., Cui D. and Xue C. (2015). Synthesis and microwave absorption properties of core-shell structured Co_3O_4-PANI nanocomposites. *Journal of Nanomaterials,* **2015**(5), 1–9. https://doi.org/10.1155/2015/845983.

Yao Y., Wang Z., Han Y., Xie L., Zhao X., Shahrokhian S. and Zhu Z. (2023). Conductometric Cr_2O_3/TiO_2/Ti_3C_2Tx gas sensor for detecting triethylamine at room temperature. *Sensors Actuators B Chemistry,* **381**(4), 133412. https://doi.org/10.1016/j.snb.2023.133412.

Yin S. and Hasegawa T. (2023). Morphology control of transition metal oxides by liquid-phase process and their material development. *KONA Powder and Particle Journal,* **40**, 94–108. https://doi.org/10.14356/kona.2023015.

Yousefi S.R., Alshamsi H.A., Amiri O. and Salavati-Niasari M. (2021). Synthesis, characterization and application of Co/Co_3O_4 nanocomposites as an effective photocatalyst for discoloration of organic dye contaminants in wastewater and antibacterial properties. *Journal of Molecular Liquids,* **337**(9), 405–415. https://doi.org/10.1016/j.molliq.2021.116405.

Zha J., Wu W., Xie P., Han H., Fang Z., Chen Y. and Jia Z. (2022). Polymeric Nanocapsule Enhances the Peroxidase-like Activity of Fe_3O_4 Nanozyme for Removing Organic Dyes. *Catalysis* **12**(6), 614. https://doi.org/10.3390/catal12060614.